NANO · MICRO small
www.small-journal.com

Triphenylamine-Based Y-Shaped Self-Assembled Monolayers for Efficient Tin Perovskite Solar Cells

Shakil N. Afraj, Chun-Hsiao Kuan, Hsu-Lung Cheng, Yun-Xin Wang, Cheng-Liang Liu, Yun-Sheng Shih, Jhih-Min Lin, Yi-Wei Tsai, Ming-Chou Chen, and Eric Wei-Guang Diau**

Triphenylamine-based Y-shaped organic sensitizers, specifically TPA-MN (1), TPA-CA (2), TPAT-MN (3), and TPAT-CA (4), are synthesized and utilized as *p*-type self-assembled monolayers (SAMs) for tin-based perovskite solar cells (TPSCs). These SAMs are developed using low-cost starting materials, primarily from triphenylamine (TPA) components. An extensive analysis is conducted to examine the crystalline, morphological, thermal, optical, electrochemical, and optoelectronic characteristics of SAMs 1–4, and the results are compared. A two-step method is employed to successfully develop tin perovskite layers on all four SAM surfaces. The resulting devices demonstrates PCE in the following order: TPAT-CA (8.1%) > TPAT-MN (6.1%) > TPA-MN (5.0%) > TPA-CA (4.2%). The TPAT-CA molecule, which contains a thiophene spacer, performed better than the other three SAMs in terms of rapid hole extraction rate, high hole mobility, and retarded charge recombination. Consequently, SAM TPAT-CA exhibited the highest device performance with excellent stability over time, retaining ≈90% from the beginning values after storage for 3000 h. The innovative Y-shaped SAMs describe in this study, characterized by their simple and efficient design, have the potential to contribute significantly to the advancement of perovskite photovoltaics, particularly in the development of cost-effective TPSC technology.

1. Introduction

Given that solar energy offers the greatest promise for carbon-free energy, developing and implementing advanced, economically feasible, and tremendously efficient solar cells is viewed as a successful strategy for transforming sunlight into electricity.[1–3] Perovskite solar cells (PSCs) have immense potential to replace traditional energy sources and fulfill the need for carbon-free electricity in the future.[3,4] This is due to their exceptional performance, cost-effectiveness, low-temperature processing ability, and outstanding optoelectronic properties.[5–7] Single-junction PSCs have already attained an efficiency of power conversion (PCE) of 26.1%, which is similar to that of crystalline silicon cells,[8] indicating a favorable outlook for the practical application of PSCs in commercial use.

An excellent technique for increasing the efficiency and stability of metal-halide PSCs involves modifying the perovskite compositions,[9] controlling the crystallization kinetics,[10,11] and optimizing interfacial engineering.[12–14] Specifically, recent advancements in hole transporting materials (HTMs) used between the perovskite absorber and indium tin oxide (ITO) anode have resulted in notable improvements in the efficiency of inverted PSCs.[4,15] However, the presence of hazardous lead in Pb-PSCs continues to be a significant environmental concern.[16–19] As a result, the lead-free TPSC has emerged as an appealing alternative, achieving a PCE of 15.7%.[20] Although TPSC's performance is currently inferior

S. N. Afraj, Y.-X. Wang, M.-C. Chen
Department of Chemistry
National Central University
No. 300 Zhongda Rd., Taoyuan 320317, Taiwan
E-mail: mcchen@ncu.edu.tw

C.-H. Kuan, H.-L. Cheng, Y.-S. Shih, E. W.-G. Diau
Department of Applied Chemistry and Institute of Molecular Science
National Yang Ming Chiao Tung University
1001 Ta-Hseuh Rd., Hsinchu 300093, Taiwan
E-mail: diau@nycu.edu.tw

The ORCID identification number(s) for the author(s) of this article can be found under https://doi.org/10.1002/smll.202408638

DOI: 10.1002/smll.202408638

C.-H. Kuan, E. W.-G. Diau
Center for Emergent Functional Matter Science
National Yang Ming Chiao Tung University
1001 Ta-Hseuh Rd., Hsinchu 300093, Taiwan

C.-L. Liu
Department of Materials Science and Engineering
National Taiwan University
No. 1, Sec. 4, Roosevelt Rd., Taipei 106319, Taiwan

J.-M. Lin, Y.-W. Tsai
National Synchrotron Radiation Research Center
Hsinchu Science Park
101 Hsin-Ann Road, Hsinchu 300092, Taiwan

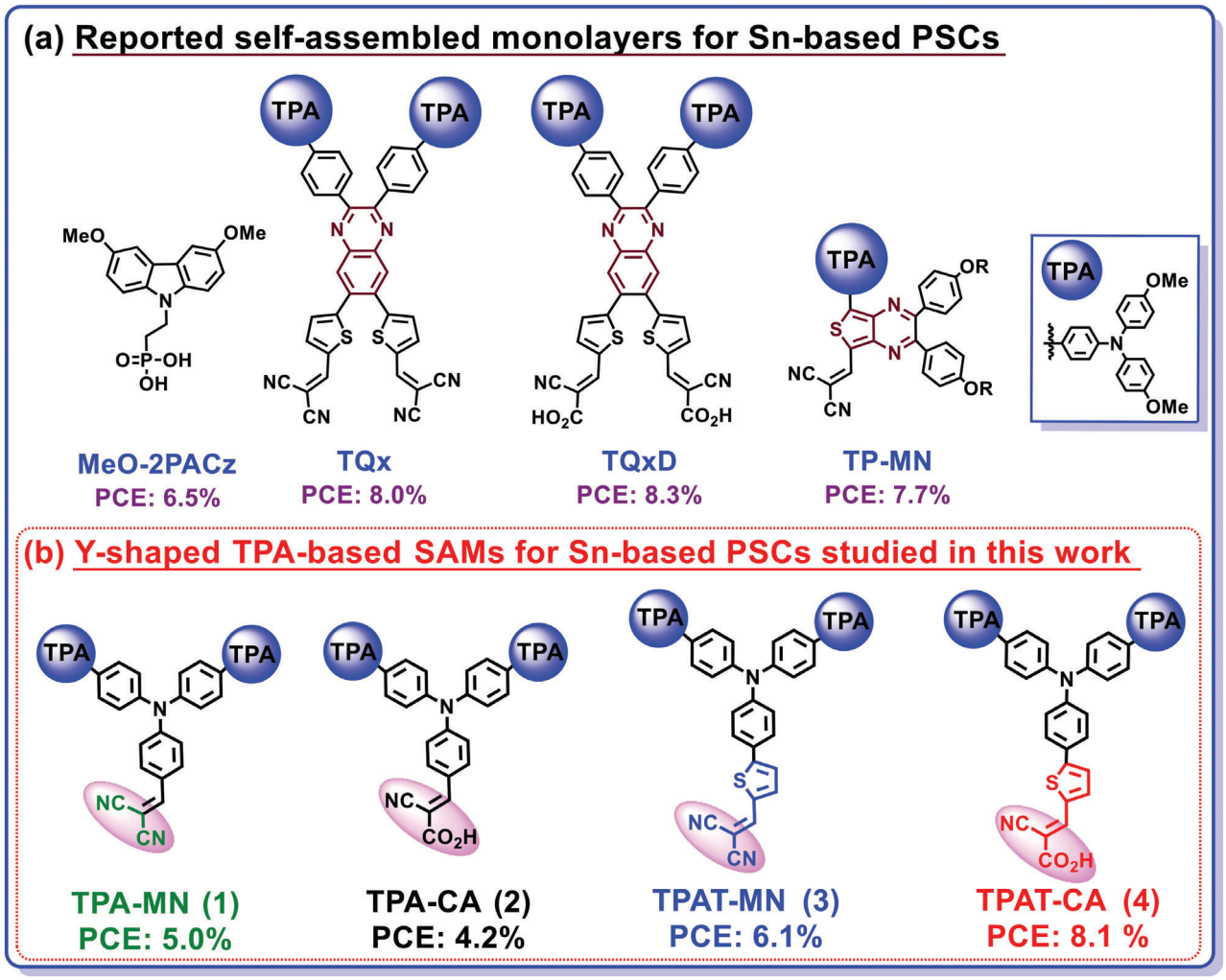

Figure 1. a) The chemical structures of the SAMs that have been reported for TPSCs; b) Triphenylamine-based Y-shaped SAMs for TPSCs studied in this work.

to its lead-based counterpart, the lower band gap of TPSC suggests a higher theoretical PCE compared to Pb-PSC. To optimize the performance of TPSCs, many strategies have been investigated, including the development of new HTMs, reduction of Sn^{2+}/Sn^{4+} oxidation, surface passivation of defects, and manipulation of crystal formation in TPSCs.[21–26]

Presently, PEDOT: PSS has served as HTM for high-performance TPSCs, and the tin perovskite layer was fabricated using a single-step technique.[27–30] Because the reaction of SnI_2 with FAI (where FA represents formamidinium) is rapid, the hydrophilic HTM, such as PEDOT: PSS, is required to facilitate rapid nucleation.[31] Due to the hygroscopic nature of PEDOT:PSS, the performance and stability of the device can be easily hindered in a humid atmosphere. To substitute hydrophilic PEDOT: PSS with other HTMs that offer good stability and well-aligned energy levels with tin perovskites, a deposition with two steps approach using hydrophobic HTMs like PTAA was successfully developed.[32–36]

Self-assembled monolayers (SAMs) are another candidate to replace PEDOT:PSS as highly efficient HTMs because of their advantageous characteristics, involving the ability to easily tune energy level alignment with perovskite, the parasitic absorption reduction, and in particular, the inexpensive and scalable production.[36–40] Typically, these SAMs structures include an anchor group that interacts with ITO substrates, an adjustable spacer that allows molecular rotation for better SAM arrangement and stacking, and a functional head group that aids in efficient hole extraction from PSC layers.[41] In inverted TPSCs, highly efficient SAMs will stand on the ITO anode to reduce charge transport losses, resulting in increased short-circuit current density (J_{SC}) and open-circuit voltage (V_{OC}). As a result, these TPSCs exhibit high PCEs and exceptional durability in single-junction,[42,43] tandem,[44] and flexible Pb-based PSCs.[45]

To achieve the best performance in highly efficient PSCs, it is necessary to have a densely packed SAMs with few imperfections. This is important because it prevents direct contact across the active layer and the electrode, resulting in increased hole extraction and retarded charge carrier recombination at the interface.[46] Despite significant progress in finding new SAMs for lead-based

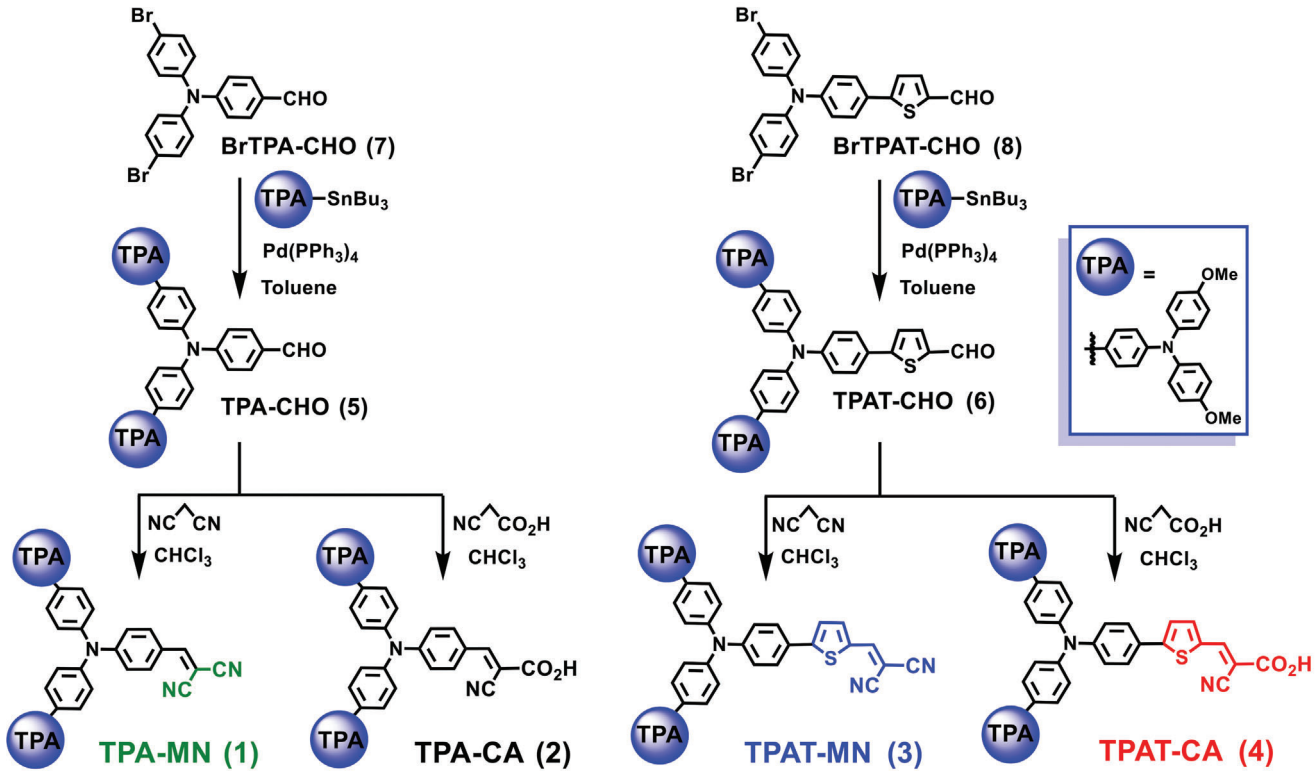

Scheme 1. Synthetic routes of Y-shaped SAMs **1–4**.

perovskite solar cells (PSCs),[15,47,48] there is a strong need to develop new SAMs for tin-based PSCs that are less harmful.

Initially, our team investigated the use of carbazole-based SAMs with **MeO-2PACz** and successfully obtained a PCE of 6.5% for TPSC.[36] Subsequently, novel SAMs based on quinoxaline were synthesized. Among them, **TQx** and **TQxD** exhibited PCEs of 8.0% and 8.3%, respectively, under the most favorable conditions for TPSC.[49] Recently, thienopyrazine-based SAMs were synthesized and applied on a NiOx film for TPSC using a two-step process.[50] The TP-MN/NiOx HTM demonstrated a significant PCE of 7.7% (**Figure 1a**).

The triphenylamine (TPA) group, extensively used as a donor unit in the preparation of organic HTMs for Pb-based PSCs, is known for its beneficial electrochemical, photophysical, and photochemical properties, cost-effective synthesis, and excellent photovoltaic performance.[51] However, the potential of using inexpensive TPA as a primary framework for creating economical organic SAMs for highly efficient TPSCs has not yet been investigated. Herein, a TPA moiety is utilized as the central core, incorporating with two electron-rich methoxy-TPA donors at its apexes, and anchored with CN/CN and CN/COOH groups at the other end to afford four Y-shaped TPA-based SAMs for the first time, labeled as **TPA-MN (1)**, **TPA-CA (2)**, **TPAT-MN (3)**, and **TPAT-CA (4)**, and their structures are shown in Figure 1b. As per our expectation, the innovative Y-shaped SAMs efficiently interact with the perovskite layer, enabling rapid photo-induced charge transfer and efficient hole injection toward the ITO substrate, resulting in enhanced PCEs up to 8.1% for TPSC.

2. Results and Discussion

Scheme 1 depicts the synthesis approaches for SAM **1–4**. The potential precursors **7** and **8** were synthesized according to the experimental procedure reported elsewhere.[52–54] The key aldehydes **TPA-CHO** (**5**) and **TPAT-CHO** (**6**) were obtained by Stille-coupling of dibromo-intermediates **7** and **8** with tin-compound in the satisfactory yields (85%). Knoevenagel condensation of aldehydes **5–6** with propanedinitrile using pyridine in chloroform generates molecules **TPA-MN** (**1**) and **TPAT-MN** (**3**) in high yields (≈78%). Similarly, Knoevenagel condensation of aldehydes **5–6** with cyanoacetic acid/piperidine in chloroform furnishes the target compounds **TPA-CA** (**2**) and **TPAT-CA** (**4**) in good yields (≈71%).

Furthermore, because of the inclusion of methoxy-TPA moiety and end-capping units (CN/COOH or CN/CN), the novel molecules **1–4** are highly soluble in common organic solvents. The chemical structures of **1–4** were verified with ^{1}H and ^{13}C NMR and other techniques (see Supporting Information). Moreover, molecules **1–4** can be readily synthesized from affordable starting materials, and the cost of compound **4** has been estimated to be \$54 g^{-1} (see Scheme S2 and Table S1 of the Supporting Information). The physical and electrochemical characteristics of **1–4** are displayed in **Table 1**. Thermogravimetric analysis (TGA; Figure S1, Supporting Information) confirmed that molecules **1–4** are thermally stable, having 5% weight loss at 249, 196, 225, and 254 °C, respectively, for **1–4**. The TGA results indicate that molecule **4**, which has rigid TPA frameworks connected to the thiophene unit with the

Table 1. Thermal, optical, and electrochemical characteristics of **1–4**.

SAM	T_d [a] [°C]	λ_{onset} [b] [nm]	E_{ox} [c] [V]	HOMO [d] [eV]	LUMO [e] [eV]	$\triangle Eg$ [f] [eV]
TPA-MN (1)	249	572	0.82	−5.26	−3.09	2.17
TPA-CA (2)	196	529	0.82	−5.26	−2.92	2.34
TPAT-MN (3)	225	625	0.82	−5.26	−3.28	1.98
TPAT-CA (4)	254	572	0.80	−5.24	−3.09	2.15

[a] By TGA; [b] UV-vis spectra were measured in *o*-$C_6H_4Cl_2$. λ_{onset} = onset absorption; [c] By DPV in *o*-$C_6H_4Cl_2$ at 25 °C. All potentials reported to Fc/Fc^+ internal reference (at +0.64 V); [d] Using E(eV) = − (4.44 + E_{ox} (vs NHE)); [e] Calculated using equation; E(eV) = HOMO + $\triangle E_g$; [f] Optical band gap calculated by 1240/λ_{onset}.

CN/COOH anchoring group, exhibits superior thermal stability compared to molecule **3**. The UV–vis spectrum (**Figure 2a**) of molecule **1** in *o*-$C_6H_4Cl_2$ is significantly red-shifted by 43 nm (λ_{onset} = 572 nm) as compared to **2** (λ_{onset} = 529 nm). Similarly, the UV–vis absorption spectrum of compound **3** in *o*-$C_6H_4Cl_2$ is also highly redshifted by 49 nm (λ_{onset} = 625 nm) compared to molecule **4** (λ_{onset} = 576 nm). This indicates that the presence of electron-deficient groups (CN/CN) in molecules **1** and **3** affects their optical properties differently from molecules **2** and **4**, which are linked to CN/COOH anchoring groups.[49]

In addition, the short wavelength absorption (~350 nm) was attributed to localized π–π^* transitions, whereas the extended wavelength absorption (529–570 nm for **1–4**) was assigned to intramolecular charge transfer (ICT) states. The electrochemical characteristics of **1–4** were derived by employing differential pulse voltammetry (DPV) in *o*-$C_6H_4Cl_2$ at 25 °C (Figure 2b). Oxidation potentials of **1–4** were calibrated using internal standard ferrocene, set at +0.64 V (*vs* NHE). The HOMO levels of SAMs **1–4** were estimated by E(eV) = −(4.44 + E_{ox}) equation (*vs* NHE). The oxidation peaks of molecules **1–4** occur at potentials of +0.82, +0.82 V, +0.82 V, and +0.80 V, respectively. Consequently, the estimated E_{HOMOs} of SAMs **1–4** are −5.26, −5.26, −5.26, and −5.24 eV, respectively. The results suggest that the two electron-deficient/anchoring groups (CN/CN or CN/COOH) exert a comparable downward influence on the electrochemical characteristics of the Y-shaped TPA-based SAMs series. SAM **4**, with extended π-conjugation, exhibited the slightly higher E_{HOMO} compared to SAMs **1–3**.[49] Next, the calculated optical bandgaps of **1–4** were in the sequence of **3** (1.98 eV) < **4** (2.15 eV) < **1** (2.17 eV) < **2** (2.34 eV). As anticipated, the inclusion of an additional thiophenyl spacer in SAMs **3** and **4** results in lower energy gaps compared to **1** and **2**. This trend aligns with the values obtained from DFT calculations (see below). The LUMO levels are calculated by equation; (E(eV) = HOMO + $\triangle E_g$), and thus values estimated are −3.09, −2.92, −3.28, and −3.09 eV for **1–4** molecules, respectively.

Furthermore, the Gaussian 03W software was used to compute DFTs for **1–4** (Figure 2c) to get insights into the structural geometry of these new SAMs. The HOMOs of **1–4** are mainly situated on the two methoxy-TPA units and the central TPA backbone. The LUMOs are located on the phenyl unit of the central TPA and the thiophene units connected to CN/COOH groups. The E_{HOMO} values obtained using DFT calculations are −4.71, −4.67, −4.66, and −4.60 eV for molecules **1–4**, respectively. The corresponding E_{LUMO} values are −2.35, −2.18, −2.70, and −2.49 eV for molecules **1–4**, respectively. The energy bandgap trend is **3** (1.96 eV) < **4** (2.11 eV) < **1** (2.36 eV) < **2** (2.49 eV) estimated by DFT, which is consistent with the UV–vis measurements.[50]

We also conducted electrostatic surface potential (ESP) surface mapping of molecules **1–4** to provide a more comprehensive understanding of the charge distribution and to identify potential areas that could interact with ITO surface (Figure 2c). The upper part of molecules **1–4** have two methoxy TPA side chains linked to the central TPA component to supply electrons to the perovskite absorber, as corroborated by DFT calculations, which show that the HOMO distributions are concentrated in the methoxy-TPA region for all SAM molecules. The lower part of molecules **1–4**, which includes either phenyl (**TPA-MN** and **TPA-CA**) or thiophene units (**TPAT-MN** and **TPAT-CA**), is linked to thiophene/benzene unit of the triphenyl/biphenyl moieties. This framework enables interaction with the ITO substrate. through the CN/COOH groups, forming a SAM for TPSC. The computational data indicate that the ESP analysis images of **1–4** show a high concentration of electrons mainly located on the cyano/carboxylic acid anchoring groups delivering a favorable environment for effective interactions between anchors and the ITO surface to form SAM.[49]

The XPS of each sample depicted in **Figure 3a–d** confirm the bonding of the molecules to the ITO substrate in the thin-film analyses. The spectra exhibit distinct features corresponding to various functional groups, including C═C, C—N, and C—O. Notably, the presence of the —COOH group is observed only in the TPA-CA and TPAT-CA samples. Subsequently, a layer of tin perovskite was applied to these substrates coated with SAMs using a previously documented two-step process.[33] Figure 3e–h depict the wettability of different SAMs. The contact angles observed for the SnI_2 precursor solution on SAM films are 15.70°, 15.25°, 14.97° and 11.86° for **TPA-MN**, **TPA-CA**, **TPAT-MN** and **TPAT-CA**, respectively. This surface modification significantly enhances the subsequent deposition of FAI, leading to the formation of $FASnI_3$ perovskites with the desired morphology. The increase in hydrophilicity and the impact of SAMs on solution processability and device efficiency highlight the connection between the processability of SAMs and device performance, emphasizing that only SAMs with optimal processability can achieve the highest performance levels.

The structures of tin perovskite films deposited on different SAMs were analyzed using scanning electron microscopy (SEM) and atomic force microscopy (AFM). Figure 3i–l present top-view images of the perovskite films on various SAMs. Among them, the film on SAM **TPAT-CA** (Figure 3l) exhibits larger and more uniform crystal grains compared to the other films. This observation aligns with the AFM results depicted in Figure 3m–p. The AFM images were analyzed to evaluate the surface roughness of the tin perovskites on various SAMs. The analysis revealed that the perovskites based on **TPAT-CA** had reduced film roughness compared to the other perovskites. Figure S2 (Supporting Information) presents AFM images and Kelvin Probe Force Microscopy (KPFM) data of SAMs on ITO substrates. The surface roughness measurements for ITO coated with SAMs **TPA-MN**, **TPA-CA**, **TPAT-MN**, and **TPAT-CA** are 3.42 nm, 3.46 nm, 3.22 nm, and 3.40 nm, respectively; the corresponding surface potentials are 2.64, 2.47, 2.64, and 3.14 mV, respectively.

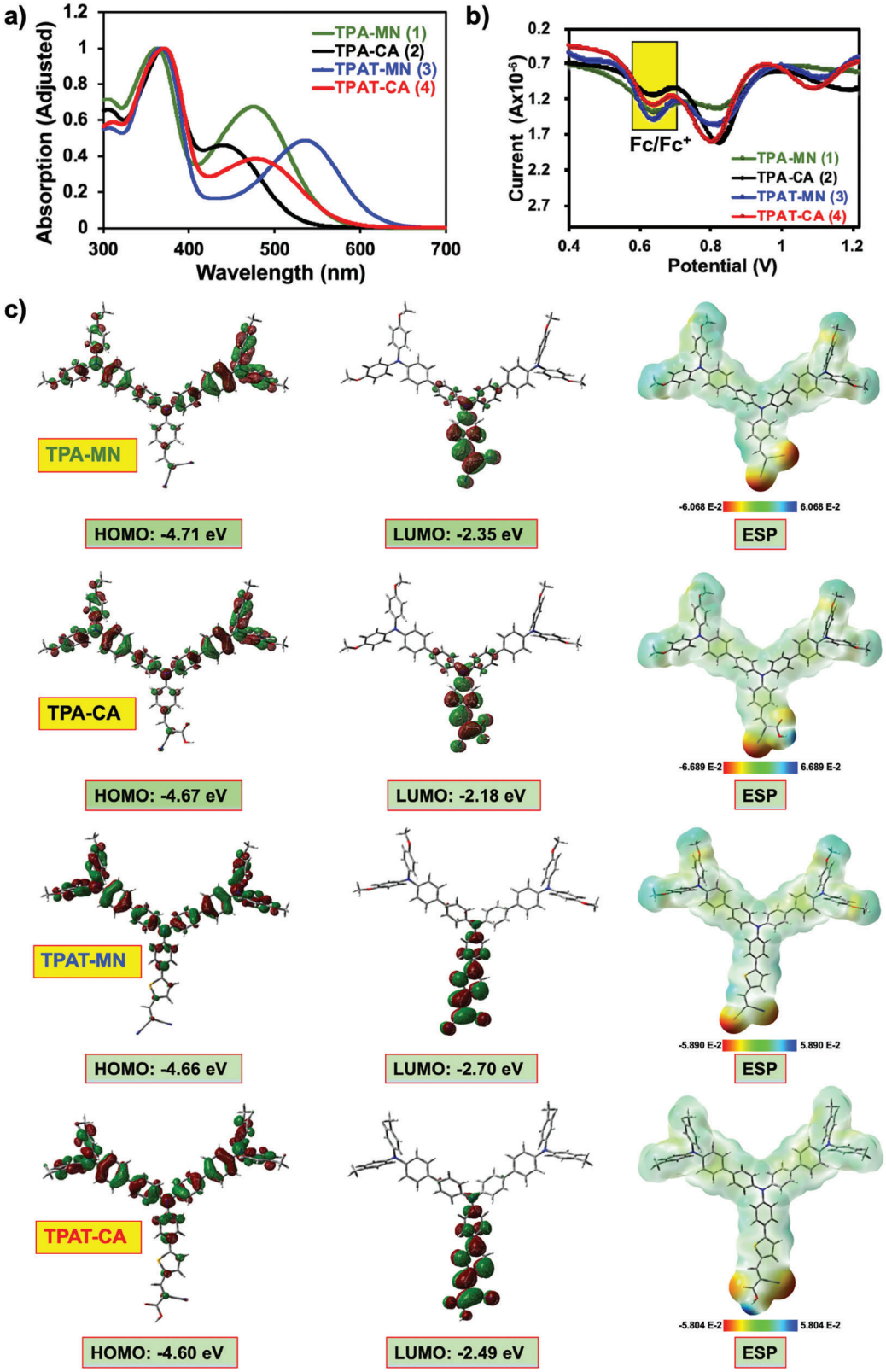

Figure 2. a) UV–vis spectra of **1**–**4** in *o*-$C_6H_4Cl_2$; (b) DPV response curves of **1**–**4**; (c) DFT and ESP analysis of **1**–**4**.

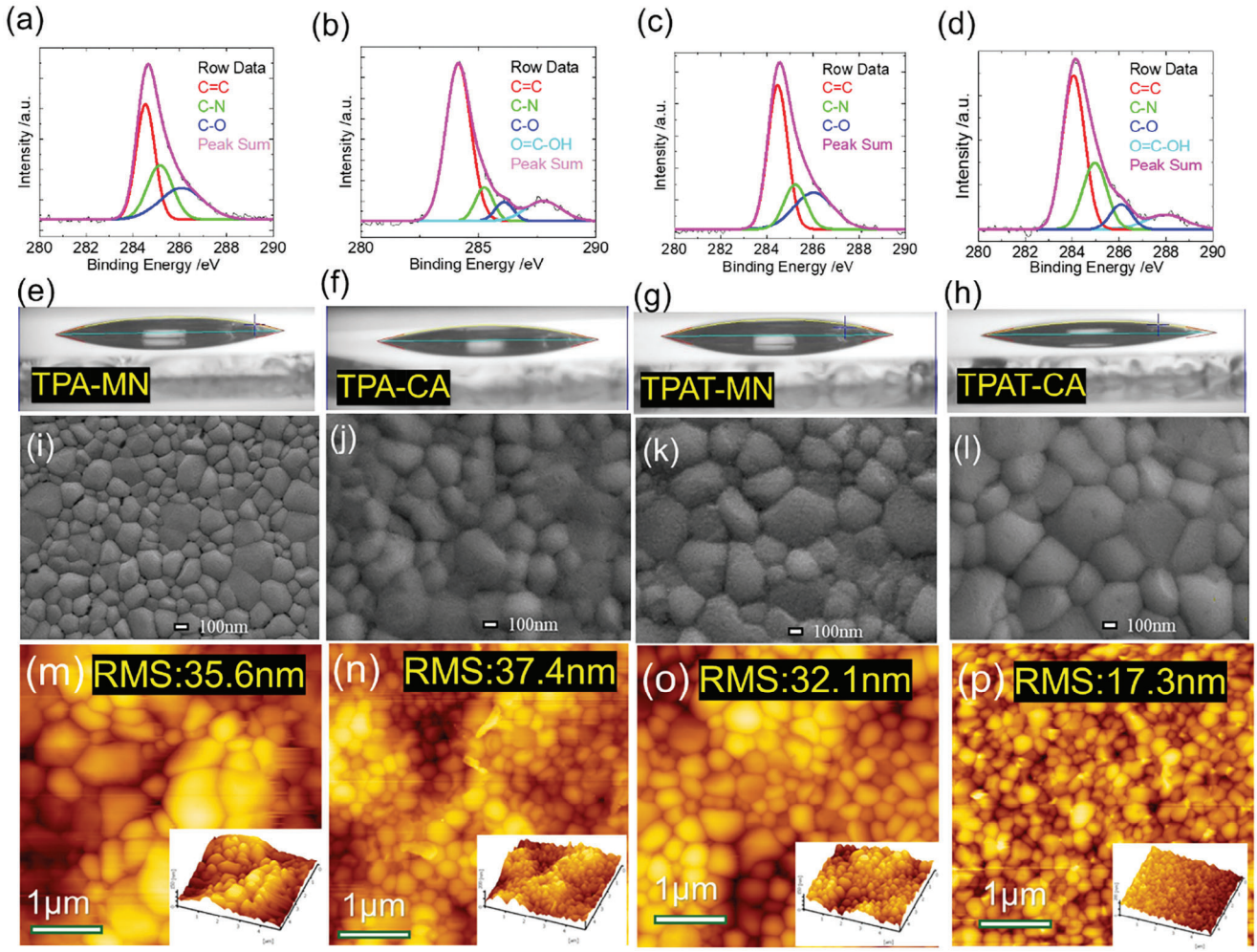

Figure 3. a–d) XPS spectra of SAMs **1–4**; e–h) contact angles of the perovskite precursor SnI_2 on various substrates as indicated; i–l) top-view SEM images of the respective perovskite films on these substrates; m–p) AFM images of the same perovskite films on different substrates showing the roughness values.

Figure 4a depicts the X-ray diffraction (XRD) patterns of perovskite nanocrystals synthesized using four distinct SAM substrates. These XRD patterns highlight the remarkable quality of the **TPAT-CA** film in terms of crystal structure. The crystallinity and perovskite arrangement in the **TPAT-CA** film, which enhances carrier transport and device performance, are confirmed by grazing incidence wide-angle X-ray scattering (GIWAXS) image (Figure 4b).

Regarding optical characteristics, Figure 4c illustrates the UV–vis absorption and PL spectra of the four perovskite films, showing comparable band gaps and PL peaks for all samples. The TC-SPC results are shown in Figure 4d, where the temporal profiles of PL are modeled using a bi-exponential decay function. The fitted kinetic parameters are presented in Table S2 (Supporting Information). The results indicate the order of SAMs in terms of hole-extraction ability as **TPAT-CA** (2.8 ns) > **TPAT-MN** (5.1 ns) > **TPA-MN** (6.6 ns) > **TPA-CA** (7.2 ns), highlighting the superior hole-extraction capacity of **TPAT-CA** SAM compared to the others.

Figure 4e displays the energy levels for all the components required to construct a TPSC. The valence band (VB) and conduction band (CB) levels of the SAM samples were identified through the analysis of Ultraviolet Photoelectron Spectroscopy (UPS) spectra (Figure S3, Supporting Information). The energy levels of the SAMs closely match those of the tin perovskite, facilitating the effective transfer of holes from the VB of the perovskite to the HOMO of the SAM, and electrons from the CB of the perovskite to the LUMO of C60. The TPSC devices were using the ITO/SAM/perovskite/C60/BCP/Ag structure, as depicted in Figure 4e. Figure 4f shows the *J*–*V* curves of the four SAM devices, with the efficiencies listed in the following order: **TPAT-CA** (8.1%) > **TPAT-MN** (6.1%) > **TPA-MN** (5.0%) > **TPA-CA** (4.2%). Table S3 (Supporting Information) provides a comprehensive comparison of the relevant photovoltaic properties. All SAM devices had comparable J_{SC}, but varied in V_{OC} and fill factor (FF), following the same order for V_{OC} vs. PCE. Figure S4 (Supporting Information) shows the IPCE spectra of the most effective devices along with the integrated current

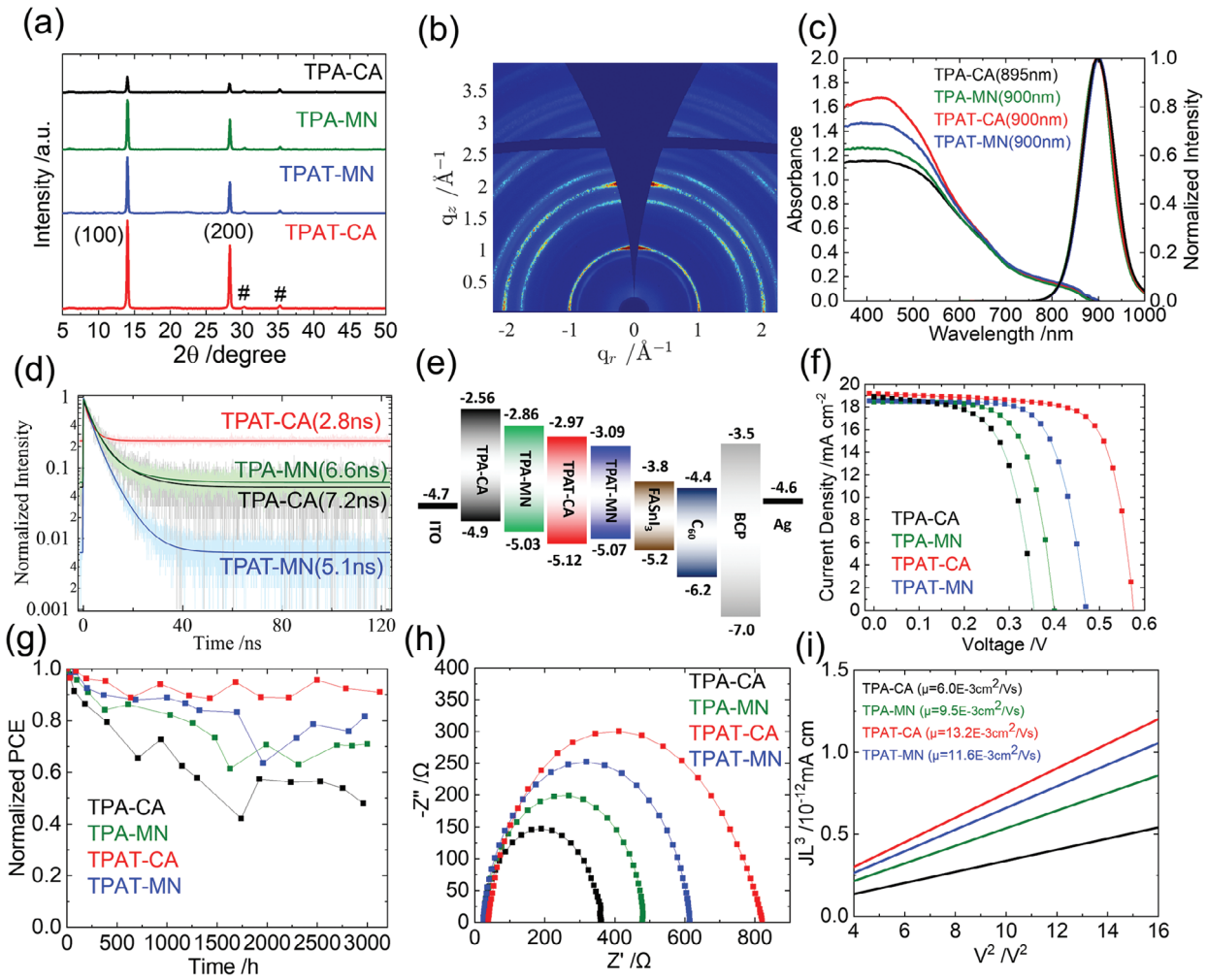

Figure 4. a) XRD of tin perovskites on different SAMs as indicated; b) GIWAXS of tin perovskite on **TPAT-CA**; c) absorption and PL spectra; d) TCSPC decay profiles of tin perovskites on various SAMs; e) the energy diagrams for TPA-SAMs; f) *J–V* curves for **TPA-CA, TPA-MN**, **TPAT-CA** and **TPAT-MN** devices; g) the long-term stability data; h) the EIS Nyquist plots; i) the space-charge limited current (SCLC) results.

density corresponding to the *J–V* scan results shown in Figure 4f. Fifteen devices were fabricated for each SAM (Tables S4–S7, Supporting Information), with performance boxplots displayed in Figure S5 (Supporting Information). Figure S6 (Supporting Information) shows the standard forward and reverse *J–V* scans for the **TPAT-CA** device, demonstrating the absence of a hysteresis effect. Figure 4g demonstrates the extended durability of the four devices stored in a glovebox under dark conditions, with the **TPAT-CA** device maintaining over 90% of its initial efficiency for more than 3000 h. In ambient air without encapsulation, the **TPAT-CA** device maintained efficiencies above 85% for 5 h at the maximum power point (MPP) under one-sun illumination, as shown in Figure S7 (Supporting Information).

To investigate the superior performance of the **TPAT-CA** device compared to the others, we conducted electrochemical impedance spectroscopy (EIS) measurements on all four devices under open-circuit conditions with the bias voltage at V_{OC} in the absence of light. The Nyquist plots for the devices display distinct semicircular characteristics shown in Figure 4h. The models were constructed using a single RC equivalent circuit model, where the resistance represents the charge recombination process. The recombination resistance followed the sequence **TPAT-CA > TPAT-MN > TPA-MN > TPA-CA**, consistent with the trend in V_{OC} and FF. Furthermore, the four SAM films underwent space-charge-limited current (SCLC) measurements to evaluate charge mobility. According to the Mott-Gurney law,[55] the SCLC plots in Figure 4i show that hole mobility follows the order: **TPAT-CA > TPAT-MN > TPA-MN > TPA-CA**. This is consistent with TCSPC, EIS, and device performance measurements. Thus, the exceptional efficiency of the **TPAT-CA** device can be attributed to minimal charge recombination (evaluated through EIS), improved hole mobility (evaluated through SCLC), and outstanding hole-extraction capability (evaluated through TCSPC), as demonstrated in the respective studies. Our findings indicate that both the cyano group and carboxylic acid are effective in connecting the SAM molecules to the ITO substrate. Additionally, the thiophene unit in this series of SAMs plays a crucial role, as demonstrated in the success of the **TPAT-CA** and **TPAT-MN** devices.

3. Conclusion

Four Y-shaped TPA-based molecules, namely **TPA-MN**, **TPA-CA**, **TPAT-MN**, and **TPAT-CA**, were synthesized and used as SAMs to replace the commonly used PEDOT:PSS as HTM in the fabrication of TPSC using a two-step technique. The CN/CN or CN/COOH anchors are chemically linked to the phenyl ring (**TPA-MN** and **TPA-CA**) or thiophene unit (**TPAT-MN** and **TPAT-CA**). These groups are potential anchoring locations for bonding with the ITO surface. Additionally, the two methoxy-triphenylamine groups are connected to the central TPA to efficiently donate electrons to the perovskite layer. These connections have been verified through DFT calculations. Our research discovers that both cyano and carboxylic acids groups serve as effective anchoring groups for the four organic molecules to create a SAM on the ITO surface. Moreover, the presence of the thiophene group in **TPAT-MN** and **TPAT-CA** is essential for the formation of tin perovskite nanocrystals with outstanding characteristics in terms of morphology, crystallinity, and surface roughness. The SAM devices demonstrate varying performance levels in terms of PCE, with **TPAT-CA** exhibiting the highest PCE (8.1%), followed by **TPAT-MN** (6.1%), **TPA-MN** (5.0%), and **TPA-CA** (4.2%). These results align with the trends observed in hole mobility (SCLC), charge recombination rate (EIS), and hole-extraction rate (TCSPC). It is noteworthy that the device constructed using Y-shaped **TPAT-CA** as a SAM with a PCE of 8.1% outperforms the device built with a carbazole-based SAM (6.5%) reported in another study.[36] Additionally, the performance of the Y-shaped TPAT-CA device is comparable to that of a device made with an X-shaped quinoxaline-based material (8.3%).[49] Currently, this is the most superior device based on SAM for TPSC, offering the benefits of cost-efficiency and having anchoring single-handed CN/COOH groups. **TPAT-CA** SAM devices exhibited exceptional and enduring stability, maintaining ≈90% of their initial performance values during 3000 h of shelf storage. Therefore, our study provides valuable insights for the development of more sophisticated SAM molecules to be used for TPSCs.

Supporting Information

Supporting Information is available from the Wiley Online Library or from the author.

Acknowledgements

S.N.A. and C.-H.K. contributed equally to this work. The authors thank Prof. C. S. Lin and Ms. Y. T. Lee of the Instrumentation Center, National Taiwan University for FEG-SEM experiments. M.-C. Chen gratefully acknowledges the funding provided by the Ministry of Science and Technology of Taiwan (MOST 111-2113-M-008-004-MY3). E. W.-G. Diau thanks to the support by the National Science and Technology Council (NSTC), Taiwan (NSTC 112-2639-M-A49-001-ASP) and the Center for Emergent Functional Matter Science of National Yang-Ming Chiao Tung University (NYCU) from The Featured Areas Research Center Program within the framework of the Higher Education Sprout Project by the Ministry of Education (MOE) in Taiwan. The authors thank Dr. Y.-W. Tsai and Dr. J.-M. Lin (TPS 25A1, NSRRC) for their kind assistance in GIWAXS data analysis. The authors also thank Dr. B.-H. Liu and Dr. C-H. Wang (TLS 24A1, NSRRC) for their kind assistance in UPS data analysis.

Conflict of Intereset

The authors declare no conflict of interest.

Data Availability Statement

Research data are not shared.

Keywords

self-assembled monolayers, tin perovskite, triphenylamine, Y-shaped

Received: September 28, 2024
Revised: October 16, 2024
Published online: November 16, 2024

[1] J. Zhou, L. Tan, Y. Liu, H. Li, X. Liu, M. Li, S. Wang, Y. Zhang, C. Jiang, R. Hua, W. Tress, S. Meloni, C. Yi, *Joule* **2024**, *8*, 1691.
[2] S. Xiong, F. Tian, F. Wang, A. Cao, Z. Chen, S. Jiang, D. Li, B. Xu, H. Wu, Y. Zhang, H. Qiao, Z. Ma, J. Tang, H. Zhu, Y. Yao, X. Liu, L. Zhang, Z. Sun, M. Fahlman, J. Chu, F. Gao, Q. Bao, *Nat. Commun.* **2024**, *15*, 5607.
[3] S. You, F. T. Eickemeyer, J. Gao, J.-H. Yum, X. Zheng, D. Ren, M. Xia, R. Guo, Y. Rong, S. M. Zakeeruddin, K. Sivula, J. Tang, Z. Shen, X. Li, M. Grätzel, *Nat.Energy* **2023**, *8*, 515.
[4] F. H. Isikgor, S. Zhumagali, L. V. T. Merino, M. De Bastiani, I. McCulloch, S. D. Wolf, *Nat. Rev. Mater.* **2023**, *8*, 89.
[5] S. D. Stranks, G. E. Eperon, G. Grancini, C. Menelaou, M. J. P. Alcocer, T. Leijtens, L. M. Herz, A. Petrozza, H. J. Snaith, *Science* **2013**, *342*, 341.
[6] Z. Xiao, Z. Song, Y. Yan, *Adv. Mater.* **2019**, *31*, 1803792.
[7] B. Chen, S.-W. Baek, Y. Hou, E. Aydin, M. De Bastiani, B. Scheffel, A. Proppe, Z. Huang, M. Wei, Y.-K. Wang, E.-H. Jung, T. G. Allen, E. Van Kerschaver, F. P. García de Arquer, M. I. Saidaminov, S. Hoogland, S. De Wolf, E. H. Sargent, *Nat. Commun.* **2020**, *11*, 1257.
[8] J. Park, J. Kim, H.-S. Yun, M. J. Paik, E. Noh, H. J. Mun, M. G. Kim, T. J. Shin, S. I. Seok, *Nature* **2023**, *616*, 724.
[9] N. J. Jeon, J. H. Noh, W. S. Yang, Y. C. Kim, S. Ryu, J. Seo, S. I. Seok, *Nature* **2015**, *517*, 476.
[10] F. Li, X. Deng, Z. Shi, S. Wu, Z. Zeng, D. Wang, Y. Li, F. Qi, Z. Zhang, Z. Yang, S.-H. Jang, F. R. Lin, S. W. Tsang, X.-K. Chen, A. K. Y. Jen, *Nat. Photon.* **2023**, *17*, 478.
[11] L. Bi, Q. Fu, Z. Zeng, Y. Wang, F. R. Lin, Y. Cheng, H.-L. Yip, S. W. Tsang, A. K. Y. Jen, *J. Am. Chem. Soc.* **2023**, *145*, 5920.
[12] F. Li, A. K. Y. Jen, *Acc. Mater. Res.* **2022**, *3*, 272.
[13] F. Li, X. Deng, F. Qi, Z. Li, D. Liu, D. Shen, M. Qin, S. Wu, F. Lin, S.-H. Jang, J. Zhang, X. Lu, D. Lei, C.-S. Lee, Z. Zhu, A. K. Y. Jen, *J. Am. Chem. Soc.* **2020**, *142*, 20134.
[14] Y. Zhou, L. M. Herz, A. K. Y. Jen, M. Saliba, *Nat. Energy* **2022**, *7*, 794.
[15] Y. Yao, C. Cheng, C. Zhang, H. Hu, K. Wang, S. D. Wolf, *Adv. Mater.* **2022**, *34*, 2203794.
[16] W. Ke, P. Priyanka, S. Vegiraju, C. C. Stoumpos, I. Spanopoulos, C. M. M. Soe, T. J. Marks, M.-C. Chen, M. G. Kanatzidis, *J. Am. Chem. Soc.* **2018**, *140*, 388.
[17] S. Vegiraju, W. Ke, P. Priyanka, J.-S. Ni, Y.-C. Wu, I. Spanopoulos, S. L. Yau, T. J. Marks, M.-C. Chen, M. G. Kanatzidis, *Adv. Funct. Mater.* **2019**, *29*, 1905393.
[18] C.-H. Kuan, R. Balasaravanan, S.-M. Hsu, J.-S. Ni, Y.-T. Tsai, Z.-X. Zhang, M.-C. Chen, E. W.-G. Diau, *Adv. Mater.* **2023**, *35*, 2300681.
[19] R. Balasaravanan, C.-H. Kuan, S.-M. Hsu, E.-C. Chang, Y.-C. Chen, Y.-T. Tsai, M.-L. Jhou, S.-L. Yau, C.-L. Liu, M.-C. Chen, E. W.-G. Diau, *Adv. Energy Mater.* **2023**, *13*, 2302047.

[20] Y. Shi, Z. Zhu, D. Miao, Y. Ding, Q. Mi, *ACS Energy Lett.* **2024**, *9*, 1895.
[21] E. Jokar, H.-S. Chuang, C.-H. Kuan, H.-P. Wu, C.-H. Hou, J.-J. Shyue, E. W.-G. Diau, *J. Phys. Chem. Lett.* **2021**, *12*, 10106.
[22] X. Liu, Y. Wang, T. Wu, X. He, X. Meng, J. Barbaud, H. Chen, H. Segawa, X. Yang, L. Han, *Nat. Commun.* **2020**, *11*, 2678.
[23] E. Jokar, P.-Y. Cheng, C.-Y. Lin, S. Narra, S. Shahbazi, E. W.-G. Diau, *ACS Energy Lett.* **2021**, *6*, 485.
[24] E. Jokar, P.-H. Hou, S. S. Bhosale, H.-S. Chuang, S. Narra, E. W.-G. Diau, *ChemSusChem* **2021**, *14*, 4415.
[25] E. Jokar, Z. Y. Huang, S. Narra, C.-Y. Wang, V. Kattoor, C.-C. Chung, E. W.-G. Diau, *Adv. Energy Mater.* **2018**, *8*, 1701640.
[26] C.-M. Tsai, Y.-P. Lin, M. K. Pola, S. Narra, E. Jokar, Y.-W. Yang, E. W.-G. Diau, *ACS Energy Lett.* **2018**, *3*, 2077.
[27] X. Jiang, H. Li, Q. Zhou, Q. Wei, M. Wei, L. Jiang, Z. Wang, Z. Peng, F. Wang, Z. Zang, K. Xu, Y. Hou, S. Teale, W. Zhou, R. Si, X. Gao, E. H. Sargent, Z. Ning, *J. Am. Chem. Soc.* **2021**, *143*, 10970.
[28] E. Jokar, C.-H. Chien, A. Fathi, M. Rameez, Y.-H. Chang, E. W.-G. Diau, *Energy Environ. Sci.* **2018**, *11*, 2353.
[29] E. Jokar, C.-H. Chien, C.-M. Tsai, A. Fathi, E. W.-G. Diau, *Adv. Mater.* **2019**, *31*, 1804835.
[30] Z. Zhu, X. Jiang, D. Yu, N. Yu, Z. Ning, Q. Mi, *ACS Energy Lett.* **2022**, *7*, 2079.
[31] X. Liu, K. Yan, D. Tan, X. Liang, H. Zhang, W. Huang, *ACS Energy Lett.* **2018**, *3*, 2701.
[32] C.-H. Kuan, G.-S. Luo, S. Narra, S. Maity, H. Hiramatsu, Y.-W. Tsai, J.-M. Lin, C.-H. Hou, J.-J. Shyue, E. W.-G. Diau, *Chem. Eng. J.* **2022**, *450*, 138037.
[33] X. Liu, T. Wu, X. Luo, H. Wang, M. Furue, T. Bessho, Y. Zhang, J. Nakazaki, H. Segawa, L. Han, *ACS Energy Lett.* **2022**, *7*, 425.
[34] S. Shahbazi, M.-Y. Li, A. Fathi, E. W.-G. Diau, *ACS Energy Lett.* **2020**, *5*, 2508.
[35] R. Shang, Z. Zhou, H. Nishioka, H. Halim, S. Furukawa, I. Takei, N. Ninomiya, E. Nakamura, *J. Am. Chem. Soc.* **2018**, *140*, 5018.
[36] D. Song, S. Narra, M.-Y. Li, J.-S. Lin, E. W.-G. Diau, *ACS Energy Lett.* **2021**, *6*, 4179.
[37] B. Niu, H. Liu, Y. Huang, E. Gu, M. Yan, Z. Shen, K. Yan, B. Yan, J. Yao, Y. Fang, H. Chen, C.-Z. Li, *Adv. Mater.* **2023**, *35*, 2212258.
[38] A. Al-Ashouri, A. Magomedov, M. Roß, M. Jošt, M. Talaikis, G. Chistiakova, T. Bertram, J. A. Márquez, E. Köhnen, E. Kasparavičius, S. Levcenco, L. Gil-Escrig, C. J. Hages, R. Schlatmann, B. Rech, T. Malinauskas, T. Unold, C. A. Kaufmann, L. Korte, G. Niaura, V. Getautis, S. Albrecht, *Energy Environ. Sci.* **2019**, *12*, 3356.
[39] G. Kapil, T. Bessho, Y. Sanehira, S. R. Sahamir, M. Chen, A. K. Baranwal, D. Liu, Y. Sono, D. Hirotani, D. Nomura, K. Nishimura, M. A. Kamarudin, Q. Shen, H. Segawa, S. Hayase, *ACS Energy Lett.* **2022**, *7*, 966.
[40] E. Aktas, N. Phung, H. Köbler, D. A. González, M. Méndez, I. Kafedjiska, S.-H. Turren-Cruz, R. Wenisch, I. Lauermann, A. Abate, E. Palomares, *Energy Environ. Sci.* **2021**, *14*, 3976.
[41] I. Levine, A. Al-Ashouri, A. Musiienko, H. Hempel, A. Magomedov, A. Drevilkauskaite, V. Getautis, D. Menzel, K. Hinrichs, T. Unold, S. Albrecht, T. Dittrich, *Joule* **2021**, *5*, 2915.
[42] Q. Jiang, J. Tong, Y. Xian, R. A. Kerner, S. P. Dunfield, C. Xiao, R. A. Scheidt, D. Kuciauskas, X. Wang, M. P. Hautzinger, R. Tirawat, M. C. Beard, D. P. Fenning, J. J. Berry, B. W. Larson, Y. Yan, K. Zhu, *Nature* **2022**, *611*, 278.
[43] S. Zhang, F. Ye, X. Wang, R. Chen, H. Zhang, L. Zhan, X. Jiang, Y. Li, X. Ji, S. Liu, M. Yu, F. Yu, Y. Zhang, R. Wu, Z. Liu, Z. Ning, D. Neher, L. Han, Y. Lin, H. Tian, W. Chen, M. Stolterfoht, L. Zhang, W.-H. Zhu, Y. Wu, *Science* **2023**, *380*, 404.
[44] K. O. Brinkmann, T. Becker, F. Zimmermann, C. Kreusel, T. Gahlmann, M. Theisen, T. Haeger, S. Olthof, C. Tückmantel, M. Günster, T. Maschwitz, F. Göbelsmann, C. Koch, D. Hertel, P. Caprioglio, F. Peña-Camargo, L. Perdigón-Toro, A. Al-Ashouri, L. Merten, A. Hinderhofer, L. Gomell, S. Zhang, F. Schreiber, S. Albrecht, K. Meerholz, D. Neher, M. Stolterfoht, T. Riedl, *Nature* **2022**, *604*, 280.
[45] L. Li, Y. Wang, X. Wang, R. Lin, X. Luo, Z. Liu, K. Zhou, S. Xiong, Q. Bao, G. Chen, Y. Tian, Y. Deng, K. Xiao, J. Wu, M. I. Saidaminov, H. Lin, C.-Q. Ma, Z. Zhao, Y. Wu, L. Zhang, H. Tan, *Nat. Energy* **2022**, *7*, 708.
[46] Z. Dai, S. K. Yadavalli, M. Chen, A. Abbaspourtamijani, Y. Qi, N. P. Padture, *Science* **2021**, *372*, 618.
[47] A. Farag, T. Feeney, I. M. Hossain, F. Schackmar, P. Fassl, K. Küster, R. Bäuerle, M. A. Ruiz-Preciado, M. Hentschel, D. B. Ritzer, A. Diercks, Y. Li, B. A. Nejand, F. Laufer, R. Singh, U. Starke, U. W. Paetzold, *Adv. Energy Mater.* **2023**, *13*, 2203982.
[48] K. Almasabi, X. Zheng, B. Turedi, A. Y. Alsalloum, M. N. Lintangpradipto, J. Yin, L. Gutiérrez-Arzaluz, K. Kotsovos, A. Jamal, I. Gereige, O. F. Mohammed, O. M. Bakr, *ACS Energy Lett.* **2023**, *8*, 950.
[49] S. N. Afraj, C.-H. Kuan, J.-S. Lin, J.-S. Ni, A. Velusamy, M.-C. Chen, E. W.-G. Diau, *Adv. Funct. Mater.* **2023**, *33*, 2213939.
[50] C.-H. Kuan, S. N. Afraj, Y.-L. Huang, A. Velusamy, C.-L. Liu, T.-Y. Su, X. Jiang, J.-M. Lin, M.-C. Chen, E. W.-G. Diau, *Angew. Chem., Int. Ed.* **2024**, 202407228.
[51] A. Farokhi, H. Shahroosvand, G. D. Monache, M. Pilkington, M. K. Nazeeruddin, *Chem. Soc. Rev.* **2022**, *51*, 5974.
[52] Y. Yang, K. Shen, J.-z. Lin, Y. Zhou, Q.-y. Liu, C. Hang, H. N. Abdelhamid, Z.-q. Zhang, H. Chen, *RSC Adv.* **2016**, *6*, 45475.
[53] Z.-M. Ju, H.-L. Jia, X.-H. Ju, X.-F. Zhou, Z.-Q. Shi, H.-G. Zheng, M.-D. Zhang, *RSC Adv.* **2015**, *5*, 3720.
[54] X. Wang, Z. Li, R. Wang, G. Zhu, F. Qin, J. Chen, J. Wang, Z. Shi, Q. Cui, C. Xu, *Appl. Phys. Lett.* **2021**, *119*, 021101.
[55] O. Almora, D. Miravet, M. García-Batlle, G. Garcia-Belmonte, *Appl. Phys. Lett.* **2021**, *119*, 242107.